Available online at www.sciencedirect.com
ScienceDirect
Acta Biomaterialia 4 (2008) 1854–1864
Acta BIOMATERIALIA
www.elsevier.com/locate/actabiomat

Mechanical and in vitro performance of 13–93 bioactive glass scaffolds prepared by a polymer foam replication technique

Qiang Fu [a], Mohamed N. Rahaman [a,*], B. Sonny Bal [b], Roger F. Brown [c], Delbert E. Day [a,d]

[a] Department of Materials Science and Engineering, Missouri University of Science and Technology, Rolla, MO 65409, USA
[b] Department of Orthopaedic Surgery, University of Missouri-Columbia, Columbia, MO 65212, USA
[c] Department of Biological Sciences, Missouri University of Science and Technology, Rolla, MO 65409, USA
[d] Graduate Center for Materials Research, Missouri University of Science and Technology, Rolla, MO 65409, USA

Received 7 January 2008; received in revised form 17 April 2008; accepted 24 April 2008
Available online 4 May 2008

Abstract

A polymer foam replication technique was used to prepare porous scaffolds of 13–93 bioactive glass with a microstructure similar to that of human trabecular bone. The scaffolds, with a porosity of $85 \pm 2\%$ and pore size of 100–500 μm, had a compressive strength of 11 ± 1 MPa, and an elastic modulus of 3.0 ± 0.5 GPa, approximately equal to the highest values reported for human trabecular bone. The strength was also considerably higher than the values reported for polymeric, bioactive glass–ceramic and hydroxyapatite constructs prepared by the same technique and with the equivalent level of porosity. The in vitro bioactivity of the scaffolds was observed by the conversion of the glass surface to a nanostructured hydroxyapatite layer within 7 days in simulated body fluid at 37 °C. Protein and MTT assays of in vitro cell cultures showed an excellent ability of the scaffolds to support the proliferation of MC3T3-E1 preosteoblastic cells, both on the surface and in the interior of the porous constructs. Scanning electron microscopy showed cells with a closely adhering, well-spread morphology and a continuous increase in cell density on the scaffolds during 6 days of culture. The results indicate that the 13–93 bioactive glass scaffolds could be applied to bone repair and regeneration.

Keywords: Scaffold; Bioactive glass; Biomaterials; Cell culture; Tissue engineering

1. Introduction

The development of synthetic scaffolds and their processing into structures that have properties tailored for applications in bone repair and regeneration are becoming increasingly important, because of several shortcomings of autografts (limited supply and donor site morbidity) and allografts (immune rejection and possible transmission of pathogens). In addition to being biocompatible, scaffold materials for bone repair and regeneration should have adequate mechanical properties to support physiological loads. Tissue infiltration and facile integration of the scaffold with surrounding tissue are required for ultimate clinical application.

Some synthetic and natural polymers, such as poly(lactic acid) (PLA), poly(glycolic acid) (PGA), copolymers of PLA and PGA, and collagen are biodegradable, so the scaffold can be gradually replaced by new bone matrix synthesized by tissue-forming cells [1–4]. However, the use of degradable polymers for replacing load-bearing bones is often challenging, because of their low mechanical strength [1]. Reinforcement with particles or short fibers of hydroxyapatite (HA) or bioactive glass improves the load-bearing properties of these polymers, and provides scaffolds that are biodegradable as well as bioactive [5–7].

Bioactive glasses, glass–ceramics and ceramics are attractive scaffold materials for bone repair, because of their abilities to enhance bone formation and to bond to surrounding tissue [8,9]. Upon implantation, bioactive glasses gradually convert to HA, the main mineral constituent of bone [9–12], and are osteoconductive as well as

* Corresponding author. Tel.: +1 573 341 4406; fax: +1 573 341 6934.
E-mail address: rahaman@mst.edu (M.N. Rahaman).

1742-7061/$ - see front matter © 2008 Acta Materialia Inc. Published by Elsevier Ltd. All rights reserved.
doi:10.1016/j.actbio.2008.04.019

osteoinductive [9]. Although brittle, bioactive glass scaffolds can provide higher mechanical strength than the aforementioned polymers [13]. The silicate-based bioactive glass designated 45S5, approved for in vivo use in the USA and elsewhere, has been widely investigated for biomedical applications [9]. The 45S5 glass cannot be easily pulled into fibers because of its tendency to devitrify (crystallize). Thermal bonding (sintering) of 45S5 particles into anatomically relevant shapes requires temperatures of ~1000 °C and higher, which leads to devitrification to form a predominantly combeite crystalline phase ($Na_2O \cdot 2CaO \cdot 3SiO_2$). While devitrification does not inhibit the ability to form an HA surface layer, the rate of conversion to HA (the bioactive potential) is reduced [14,15].

Another silicate-based bioactive glass, designated 13–93, with a modified 45S5 composition [16,17], has more facile viscous flow behavior and less tendency to crystallize than 45S5. The 13–93 glass is approved for in vivo use in Europe. The glass can be pulled into fibers, and particles or short fibers have been sintered, without devitrification, to form porous scaffolds with anatomically relevant shapes, such as the human proximal tibia [13]. Porous scaffolds consisting of 13–93 fiber rafts supported the in vitro growth and differentiation of MC3T3-E1 preosteoblastic cells [18]. Quantitative measurement of DNA showed no significant difference in cell proliferation between dense disks of 45S5 and 13–93 glass [18].

Several techniques have been employed to produce porous three-dimensional scaffolds of polymers and bioactive ceramics. These methods include thermally induced phase separation (TIPS) [19,20], solid freeform fabrication [21,22], solvent casting and particle leaching [23,24], freeze-casting [25–28] and polymer foam replication [15,29–32]. Interconnected pores with a mean diameter (or width) of 100 μm or greater and open porosity of >50% are generally considered to be the minimum requirements to permit tissue ingrowth and function in porous scaffolds [33,34].

Using a foam with the appropriate architecture, scaffolds with a microstructure approximating trabecular bone can be prepared by the polymer foam infiltration technique [35]. In this technique, a polymer foam is infiltrated with a stable suspension of colloidal particles. After drying, the system is heated to decompose the polymer foam, and sintered at a higher temperature to densify the network of particles. The method has been used to prepare porous scaffolds of 45S5 glass–ceramic [15], HA [29,30], biphasic calcium phosphate [31] and akermanite [32]. The strength of the construct is critically dependent on the ability to achieve a solid network with high density. This is dependent on the particle packing of the infiltrated foam, which, in turn, is dependent on the colloid stability of the suspension used to infiltrate the foam. Generally, a stable suspension leads to a more homogeneous and higher particle packing density in the infiltrated foam, which leads to more facile densification of the particulate network.

Based on the aforementioned forming characteristics and bioactivity of 13–93 glass, coupled with the ability of the polymer foam infiltration technique to produce a bone-like microstructure, an investigation of the mechanical and in vitro performance of 13–93 glass scaffolds prepared by this technique was undertaken. The microstructure and compressive mechanical properties of the fabricated scaffolds were characterized, and the ability of the constructs to support the attachment and growth of osteoblastic cells was evaluated. The mouse MC3T3-E1 cell line chosen for these experiments has been used extensively in previous in vitro investigations of biomaterials for bone repair and tissue engineering [36,37].

2. Materials and methods

2.1. Preparation of 13–93 glass scaffolds

Glass with the 13–93 composition (wt.%) ($53SiO_2$, $6Na_2O$, $12K_2O$, 5MgO, CaO, $4P_2O_5$) was prepared by melting a mixture of analytical grade Na_2CO_3, K_2CO_3, $MgCO_3$, $CaCO_3$, SiO_2 and $NaH_2PO_4 \cdot 2H_2O$ (Fisher Scientific, St. Louis, MO) in a platinum crucible at 1300 °C and quenching between stainless steel plates. The glass was crushed in a hardened steel mortar and pestle and classified using stainless steel sieves to provide particles of size <150 μm. These particles were further ground for 2 h in an attrition mill (Model 01-HD, Union Process, Akron, OH), using high-purity Y_2O_3-stabilized ZrO_2 milling media and ethanol as the solvent, to provide particles in the colloidal size range (<5–10 μm). The average size and size distribution of the particles were measured using a laser diffraction particle size analyzer (Model LS 13 320; Beckman Coulter Inc., Fullerton, CA).

The colloidal properties of the 13–93 glass particles and the ability of different dispersants to stabilize the particles in water were investigated in order to prepare stable suspensions for use in the polymer foam replication technique. Preliminary experiments were performed to test the sedimentation behavior of suspensions (5 vol.% particles) stabilized with 0.25–2 wt.% of five different dispersants (based on the dry mass of the particles). The dispersants were ammonium polymethacrylate (Darvan C; mol. wt. = 10,000–16,000; R.T. Vanderbilt Co., Norwalk, CT), sodium polyacrylate (Darvan 811, mol. wt. = 5000; R.T. Vanderbilt Co.), poly(methylvinyl ether) (EasySperse; ISP, Wayne, NJ), Dynol 604 (Air Products & Chemicals Inc., Allentown, PA) and Targon 1128 (BK Ladenburg GmbH, Ladenburg, Germany). The suspensions were poured to a height of ~5 cm into test tubes (~3 cm in diameter × 6.5 cm) and, after vigorous shaking, allowed to settle for 24 h. The suspensions stabilized with Dynol 604 or Targon 1128 settled almost completely to give loose flocculated sediments, indicating that these two dispersants were ineffective for stabilizing the particles. On the other hand, the suspensions stabilized with EasySperse showed the least sedimentation, whereas Darvan C or Darvan 811 produced sedimentation results that were intermediate between those for EasySperse and Dynol 604 (or Targon 1128). Because of

their ineffectiveness, Dynol 604 and Targon 1128 were not used in subsequent experiments.

The zeta-potential of the particles in an aqueous medium, with or without the presence of Darvan C, Darvan 811 or EasySperse, was measured as a function of the pH of the aqueous medium using electrophoresis (Zeta-meter 3.0, Zeta-Meter Inc., NY). At each pH value, the zeta-potential was measured at least 10 times, and the results were determined as a mean ± standard deviation. To determine the concentration of dispersant for optimum stability, the viscosity of the suspension (35 vol.% particles) was measured as a function of the dispersant concentration using a rotating cylinder viscometer (VT500; Haake Inc., Paramus, NJ).

Aqueous suspensions containing 20–50 vol.% glass particles, 0.5 wt.% Easysperse as dispersant and 1 wt.% poly (vinyl alcohol) (PVA; DuPont Elvanol® 90–50) as binder were prepared by ball milling for 24 h in polypropylene bottles using Al_2O_3 as the milling media. (The concentrations of the dispersant and binder were based on the dry mass of glass powder used.) The viscosity of the suspensions vs. particle concentration was measured using a rotating cylinder viscometer (Haake VT500).

Four commercial polymer foams were examined in a scanning electron microscope (Hitachi S-4700) and the structure of each foam was compared with that of human trabecular (or cancellous) bone. On the basis of these observations, a polyurethane foam with a structure close to that of trabecular bone was selected for the present experiments. Scaffolds were prepared by infiltrating the slurry (35 vol.% particles) into the foam (9 mm in diameter × 20 mm long), so that the walls of the foam were coated with the slurry. Excess slurry was squeezed out of the foam. In the infiltration step, the immersed foam was compressed and released several times to let the slurry adhere to the walls of the polymer network. The as-coated foam was dried at room temperature for 24 h, and then subjected to a controlled heating schedule to first decompose the polymer phase and then densify the network of glass particles. The sample was heated at 1 °C min^{-1} to 500 °C in flowing O_2 gas to decompose the foam, then at 5 °C min^{-1} to 700 °C, and kept at this temperature for 1 h to densify the glass network and form a porous, cylindrical glass construct without crystallizing the glass. A diamond-coated wafering blade was used to section the porous glass cylinders into disks (6 mm in diameter × 2 mm thick) for use in cell culture experiments.

2.2. Characterization of 13–93 glass scaffolds

To assess the crystallinity of the 13–93 glass after sintering, scaffolds were ground into a powder (particle size <45 μm) and analyzed using X-ray diffraction (XRD; Rigaku, Model D/mas 2550 v) in a step-scan mode (0.05° 2θ and 2 s per step; Cu Kα radiation; $\lambda = 0.15406$ nm). For comparison, the powder of a sample of dry human trabecular bone was also analyzed using XRD. Samples of the 13–93 glass constructs and a section of dry human bone were sputter-coated with Au/Pd and examined in a scanning electron microscope (SEM; Hitachi S-4700) to compare the pore morphology of the scaffolds with that of human trabecular bone. The open porosity of the samples was measured using the Archimedes method. Pore size distribution of the accessible (open) pores was measured using mercury intrusion porosimetry (Poremaster; Quantachrome, FL) [38]. The compressive strength of cylindrical samples (6 mm in diameter × 12 mm long) was measured using an Instron testing machine (Model 4881; Instron Co., Norwood, MA) at a crosshead speed of 0.5 mm min^{-1}. Eight samples were tested, and the mean strength and standard deviation were determined.

2.3. Assessment of scaffold bioactivity

Porous scaffolds and dense disks of 13–93 glass were immersed in simulated body fluid (SBF) at 37 °C and then analyzed for the formation of a calcium phosphate layer on the glass surfaces as one indication of bioactivity. The composition of the SBF was identical to that described by Kokubo et al. [39]. Cylindrical scaffolds (6 mm in diameter × 2 mm thick) and disks (10 mm in diameter × 2 mm thick) were cleaned with ethanol in an ultrasonic bath, dried in air and placed in sealed polyethylene bottles containing 50 ml of SBF at 37 ± 2 °C. The SBF was replaced every 24 h. After a given immersion time, the scaffolds and disks were dried for at least 24 h in air at room temperature and observed in the SEM. Crystalline phases formed on the surface of the glass disks were detected using thin-film XRD at a scanning rate of 1.8°/min in the 2θ range 10–80°.

2.4. Cell culture

The established MC3T3-E1 line of mouse preosteoblastic cells was obtained from ATCC and cultured in α-MEM medium supplemented with 10% fetal bovine serum plus 100 μg ml^{-1} penicillin and 100 μg ml^{-1} streptomycin sulfate. Prior to seeding with cells, dry-heat sterilized scaffolds (6 mm in diameter × 2 mm thick) were soaked for 1 h in a 0.01% solution of polylysine (mol. wt. >150,000) to enhance cell adhesion. The pre-treated scaffolds were blotted dry, rinsed twice with phosphate-buffered saline (PBS), placed on a 6 cm diameter Teflon disk and seeded with 50,000 MC3T3-E1 cells suspended in 35 μl of complete medium. After incubation for 4 h to permit cell attachment, the cell-seeded scaffolds were transferred to a 24-well plate containing 2 ml of complete medium per well. The control group consisted of the same number of cells seeded in wells containing 2 ml of complete medium. All cell cultures were performed at 37 °C in a humidified atmosphere of 5% CO_2, with the medium changed every 2 days.

2.5. MTT detection of viable cells

Some of the cell-seeded scaffolds were placed in 400 μl serum-free medium containing 100 μg of the tetrazolium

salt MTT for the last 4 h of incubation to permit visualization of metabolically active cells on and within the porous 13–93 glass scaffolds. After the incubation, the scaffolds were briefly rinsed in PBS and blotted dry. Images of the scaffolds were obtained using a stereomicroscope fitted with a digital camera to qualitatively assess the distribution of insoluble purple formazan, a product of mitochondrial reduction of MTT by viable cells. The MTT-labeled scaffolds were then frozen at −70 °C and fractured with a cooled microtome blade, and the fracture cross-section visually examined to assess the presence of purple formazan within the interior of the scaffold.

2.6. Cell morphology

At selected culture intervals, glass scaffolds with attached cells were removed, washed twice with warm PBS and placed in 2.5% glutaraldehyde in PBS. After an overnight soak in glutaraldehyde, fixed samples were washed extensively with PBS, post-fixed with 1% osmium tetroxide in PBS for 1 h, washed repeatedly with PBS, dehydrated with a graded ethyl alcohol series and then soaked for 10 min in hexamethyldisilazane (HMDS). After a second soaking in HMDS, the samples were allowed to fully evaporate before being sputter-coated with Au/Pd. The samples were observed in an SEM at 5 kV accelerating voltage.

2.7. Quantitative protein assay

Total protein in lysates recovered from the cell-seeded scaffolds was measured with a micro-BCA Protein Assay Kit (Piece Biotechnology, Rockford, IL) to assess cell proliferation on the scaffolds. Cells were detached from the glass constructs and the control wells by lysis in 400 μl of 1% Triton solution for 1 h. Aliquots of the released lysate were mixed with 100 μl of micro-BCA working reagent and the resultant mixture incubated at 50 °C for 20 min. Sample absorbance values were measured at 550 nm in a BMG FLUORstar Optima plate reader with bovine serum albumin used as a standard for comparison.

2.8. Statistical analysis

All biological experiments (4 samples in each group) were run either in duplicate or triplicate. The data are presented as the mean ± standard deviation. Statistical analysis was performed using Student's *t*-test. Values were considered to be significantly different when $p < 0.05$.

3. Results

3.1. Particle and suspension properties

The median size (d_{50}) of the 13–93 glass particles was 2 μm, with a standard deviation of 1 μm. Fig. 1 shows data for the zeta-potential of the glass particles as a function of the pH of the aqueous suspension, for suspensions containing no dispersant and for suspensions containing Darvan 811, Darvan C or EasySperse (1.0 wt.% based on the dry mass of the glass particles). The isoelectric point (the pH at which the zeta-potential is zero) was found to be pH ≈ 3.0. When a bioactive glass is immersed in an aqueous solution, ions (such as Na^+) dissolve from the glass into the solution at different pH values [9,10], which might be expected to influence the zeta-potential of the glass particles. For silicate 45S5 bioactive glass, Hench [9] showed that the early stages of the dissolution process resulted in the formation of a silica-rich surface layer. Since the 13–93 composition is based on that of 45S5, a similar dissolution mechanism might be expected. Furthermore, the time frame for each zeta-potential measurement was <30 min, so the surface layer might correspond to that of a silicate glass. If additional changes occur, such as the formation of a calcium phosphate material on the surface of the glass particles, then changes in the zeta-potential might be expected at later times.

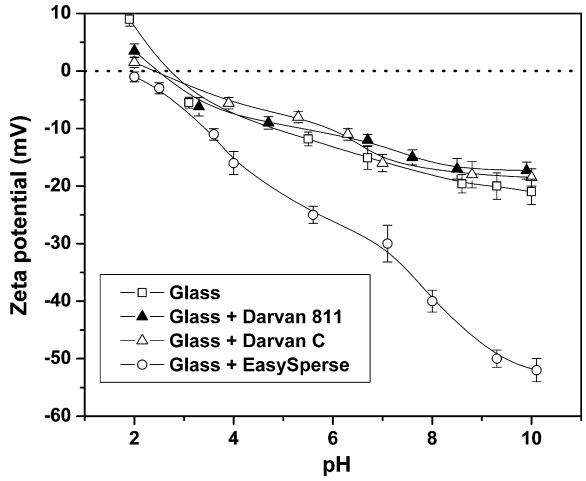

Fig. 1. Zeta-potential of 13–93 glass particles vs. pH, for suspensions without dispersant and for suspensions containing 1 wt.% Darvan 811, Darvan C or EasySperse.

Both Darvan 811 and Darvan C caused no change in the zeta-potential of the particles, which may be an indication that these two anionic dispersants were not adsorbed (or only weakly adsorbed) on to the particle surfaces. These two anionic dispersants are highly charged at pH values >4–5, due to a high degree of dissociation [38]. Significant adsorption should result in a marked change in the zeta-potential of the particles, which was not observed. On the other hand, a considerable increase in the magnitude of the zeta-potential occurred with the dispersant EasySperse, indicating that this anionic dispersant was adsorbed onto the particle surfaces. Since the higher zeta-potential was expected to provide enhanced colloidal stability of the suspension by the mechanism of electrosteric stabilization, the data indicated that EasySperse was more effective for dispersing 13–93 glass particles than Darvan C or Darvan 811.

The optimum concentration of EasySperse required to stabilize the glass particles was determined from the data for the viscosity of an aqueous suspension (35 vol.% particles) as a function of the dispersant concentration at a constant shear rate (100 s^{-1}). Fig. 2 indicated that 0.5 wt.% EasySperse gave the lowest viscosity of the suspension (~220 MPa s). Henceforth, the aqueous suspensions used in the experiments were stabilized with 0.5 wt.% EasySperse.

Fig. 3 shows the relative viscosity (shear rate = 100 s^{-1}) of the suspension as a function of glass particle concentration. The data can be fitted by a modified Krieger–Dougherty equation [40,41]:

$$\eta_r = \left(1 - \frac{\phi}{\phi_m}\right)^{-n} \quad (1)$$

where η_r, the relative viscosity, is defined as the viscosity of the suspension, η, divided by the viscosity of the solvent (water) η_L, φ is the volume fraction of particles, φ_m is the volume fraction of particles at which the viscosity becomes practically infinite and n is a fitting parameter. The maximum solids loading predicted by this model was $\varphi_m = 55$ vol.%, with $n = 3.4$. The colloid stability and viscosity of the suspension are important parameters for the preparation of scaffolds by the polymer foam replication method. Highly concentrated suspensions (>40 vol.% particles) were difficult to infiltrate homogeneously into the foam, whereas suspensions containing less than ~20 vol.%) resulted in scaffolds that were too weak for handling. A suspension containing 35 vol.% particles was selected to provide a compromise between ease of infiltration and scaffold strength.

3.2. Microstructure of 13–93 glass scaffolds

Fig. 4a shows that the microstructure of the polyurethane foam used in these experiments was generally similar to that of a sample of dry human trabecular bone (Fig. 4b).

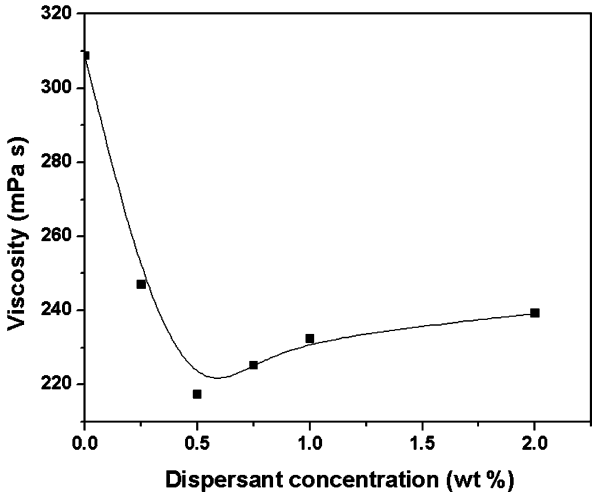

Fig. 2. Viscosity of aqueous suspensions containing 35 vol.% 13–93 glass particles vs. dispersant concentration (shear rate = 100 s^{-1}).

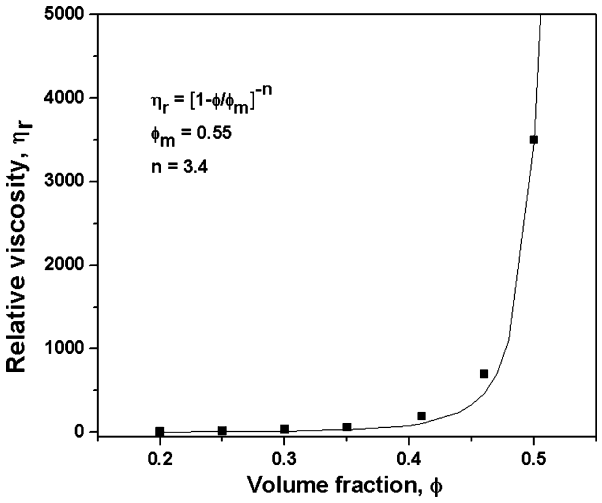

Fig. 3. Relative viscosity vs. volume fraction of 13–93 glass particles in aqueous suspensions stabilized with 0.5 wt.% EasySperse (shear rate = 100 s^{-1}).

The microstructure of a fractured cross-section of the 13–93 glass scaffold (Fig. 4c and d) consisted of a dense network of glass and interconnected cellular pores. In general, the microstructural and morphological features of the scaffold were similar to those of human trabecular bone (Fig. 4b). The solid network (50–100 μm in diameter) of the scaffold appeared to be fully dense, with a smooth surface, and the diameter of the pores was in the range 100–500 μm. At the sintering temperature used, no visible deformation of the overall shape of the scaffold occurred. The porosity of the scaffolds was 85 ± 2%. Mercury intrusion porosimetry (Fig. 5) confirmed the SEM observations that the fabricated glass constructs contained interconnected pores of size ~100–500 μm.

3.3. Mechanical properties of 13–93 glass scaffolds

The stress–strain behavior of a fabricated 13–93 glass scaffold in compression is shown in Fig. 6. The stresses and strains are the engineering values calculated from the initial cross-sectional area and length. The peaks and valleys in the curve may be related to progressive breaking of the solid particulate network. The response showed linear elastic behavior during the initial compression, followed by a decrease in stress, possibly because of the fracture of some struts in the solid network. As the strain increased, the additional struts were fractured. Finally, the macro-cracks propagated in the scaffold, leading to a decrease in stress to almost zero. The determination of the elastic modulus from compression tests is subject to several sources of error, which can lead to considerable variation. In the present experiments, the modulus determined from the initial linear region of the stress–stain curve was 3.0 ± 0.5 GPa. Taking the compressive strength as the highest stress on the stress–strain curve, the average compressive strength was 11 ± 1 MPa for eight samples tested (porosity = 85 ± 2%).

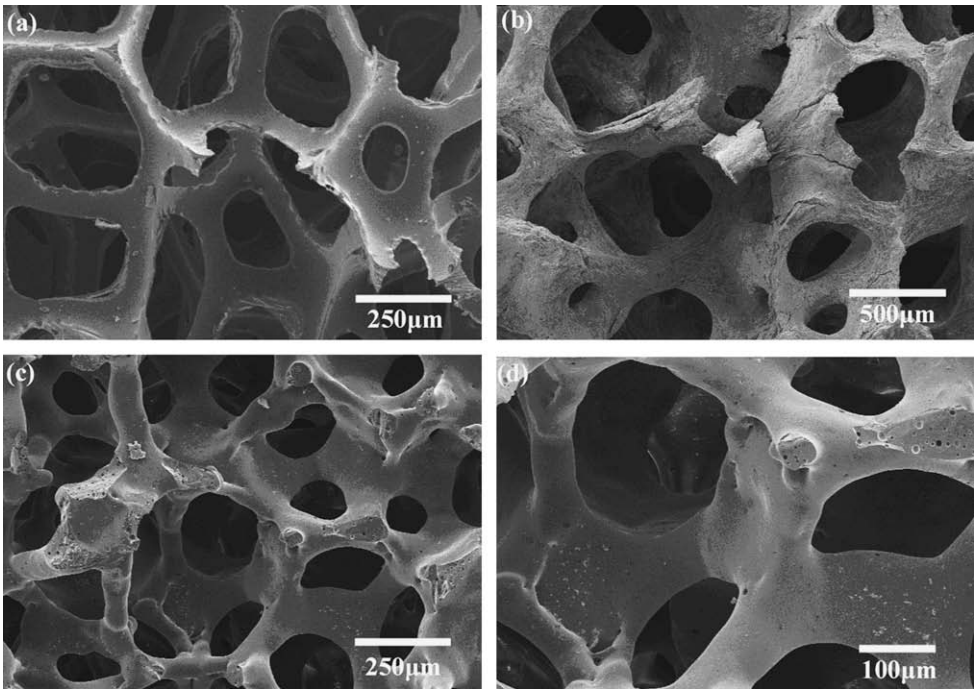

Fig. 4. Microstructures of: (a) polyurethane foam used in the experiments; (b) dry human trabecular bone; and (c, d) 13–93 glass scaffolds fabricated by a polymer foam replication technique.

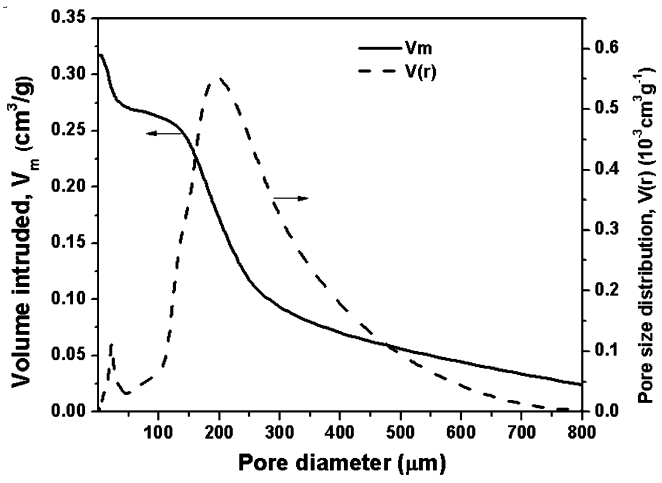

Fig. 5. Mercury porosimetry data for the pore volume and pore size distribution vs. pore radius, for the fabricated 13–93 glass scaffolds.

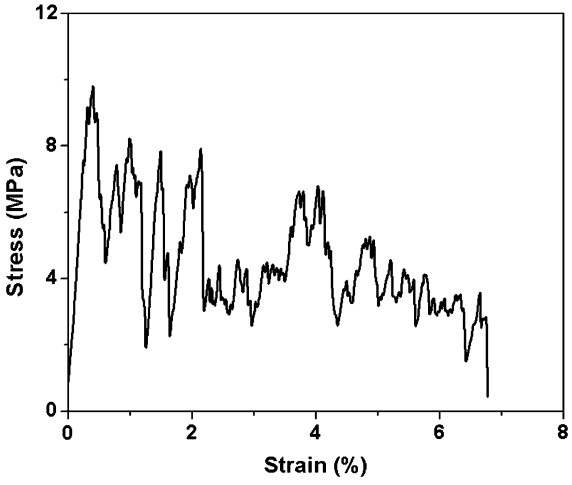

Fig. 6. Stress–strain response of porous 13–93 glass scaffolds in compression.

3.4. In vitro bioactivity

Fig. 7 shows SEM images of the surface of a 13–93 glass scaffold after immersion in an SBF for 7 days. Compared to the smooth glass surface of the as-fabricated construct (Fig. 4a and b), the treatment in the SBF produced a fine particulate surface layer. High-resolution SEM images (Fig. 7c) showed that the surface consisted of a porous network of nanometer-sized, needle-like crystals.

XRD analysis showed that the as-formed porous glass scaffolds were amorphous (Fig. 8b). The band centered at ~30° 2θ was indicative of an amorphous material. After immersion for 7 days in the SBF, the thin-film XRD pattern of the dense disks (Fig. 7c) contained peaks corresponding to those of a reference HA (JCPDS 72-1243), indicating the formation of HA on the glass surface. The width of the major peaks may be caused by X-ray line broadening due to nanometer-sized crystals, confirming the presence of the fine, needle-like crystals observed by SEM. The major peaks in the pattern also occurred at approximately the same 2θ values as those for human trabecular bone (Fig. 8d).

3.5. Cell culture

SEM images in Fig. 9 show the morphology of MC3T3-E1 cell growth on the surface of the 13–93 glass scaffolds

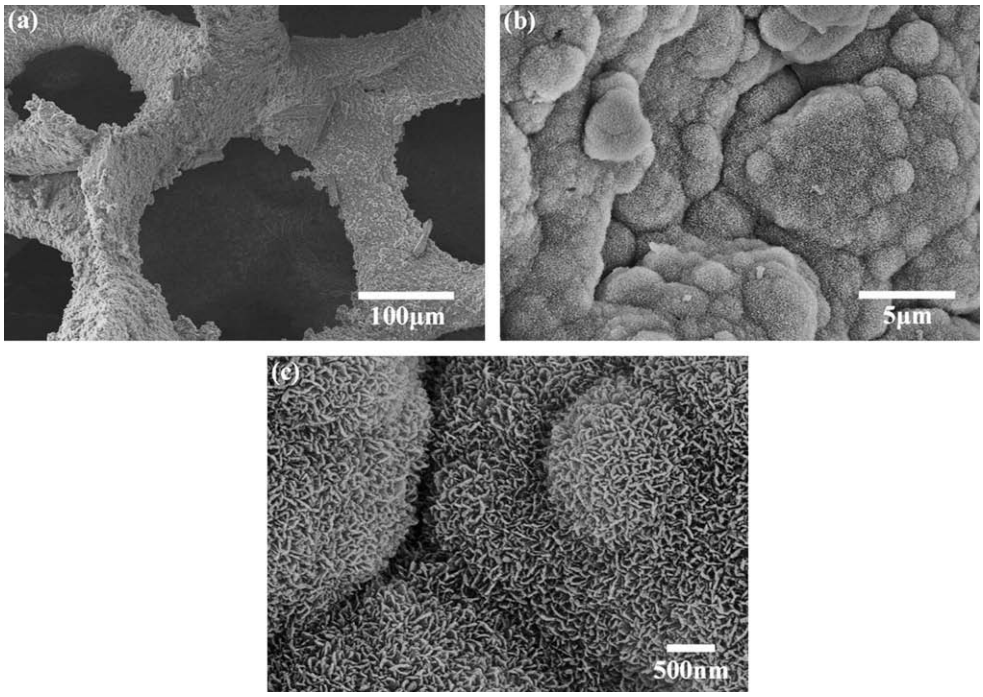

Fig. 7. SEM images of the surface of a 13–93 glass scaffold after immersion for 7 days in SBF: (a) lower magnification image; and (b, c) higher magnification image showing fine needle-like hydroxyapatite crystals.

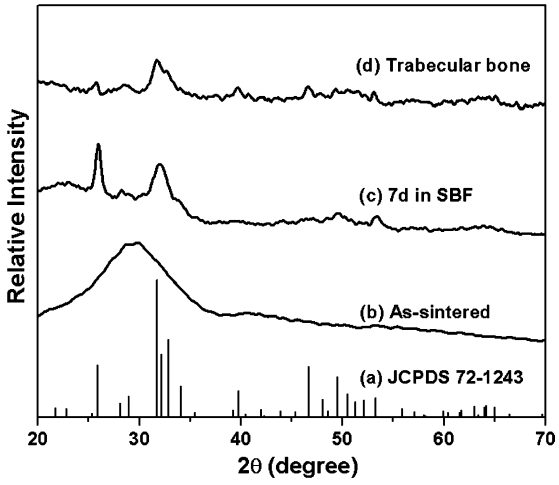

Fig. 8. X-ray diffraction patterns of: (a) reference hydroxyapatite (JCPDS 72-1243); (b) porous 13–93 glass scaffold in the as-sintered condition; (c) sintered 13–93 glass scaffold after immersion in a simulated body fluid for 7 days; and (d) human trabecular bone.

for 2, 4 and 6 days. The preosteoblastic cells visible in these micrographs were elongated and appeared to align along the long axis of the dense struts of the scaffold. The cells were well spread at all three culture intervals with numerous cytoplastic projections, and they appeared to be well attached to the surface of the constructs (Fig. 9a). The number of cells on the scaffold increased as a function of culture time (Fig. 9b). A high-magnification image (Fig. 9c) showed cell growth into pores of size <100 μm, as well as the formation of numerous cell projections, features that indicated firm cell attachment to the surface. After culturing for 6 days, almost the whole surface of the scaffold was covered with cells (Fig. 9d and e), and cell spreading on the struts was visible. The cells began to aggregate, and neighboring cells appeared to maintain physical contact with each other by multiple extensions (Fig. 9e).

Results of the quantitative assay of total protein in cell lysates recovered from the 13–93 glass scaffolds and the control wells after incubations of 2, 4 and 6 days are shown in Fig. 10. The amounts of protein recovered from the scaffolds showed a nearly linear increase in cell proliferation during the 6 day incubation, a finding that complements the progressive increase in cell density seen in the SEM images. Furthermore, the results indicated that the cell proliferation kinetics on the scaffolds were the same as those in the control wells. These data indicated that the MC3T3-E1 cells were able to grow on the 13–93 glass scaffolds at essentially the same rate as they did on the surface of plastic culture vessels.

Photographic images of cell-seeded scaffolds treated with MTT during the last 4 h of incubation are shown in Fig. 11. The purple pigment visible on the scaffold was an indication of viable cells, and was the result of mitochondrial reduction of MTT to an insoluble formazan product. The increase in intensity of the purple color with culture time indicated the proliferation of viable, metabolically active cells on the scaffold (Fig. 11a). The purple formazan visible on the freeze-fracture face of a scaffold cultured for 6 days (Fig. 11b) indicated the presence of metabolically active cells within the interior of the construct. Furthermore, the uniformly distributed purple formazan on the surface and

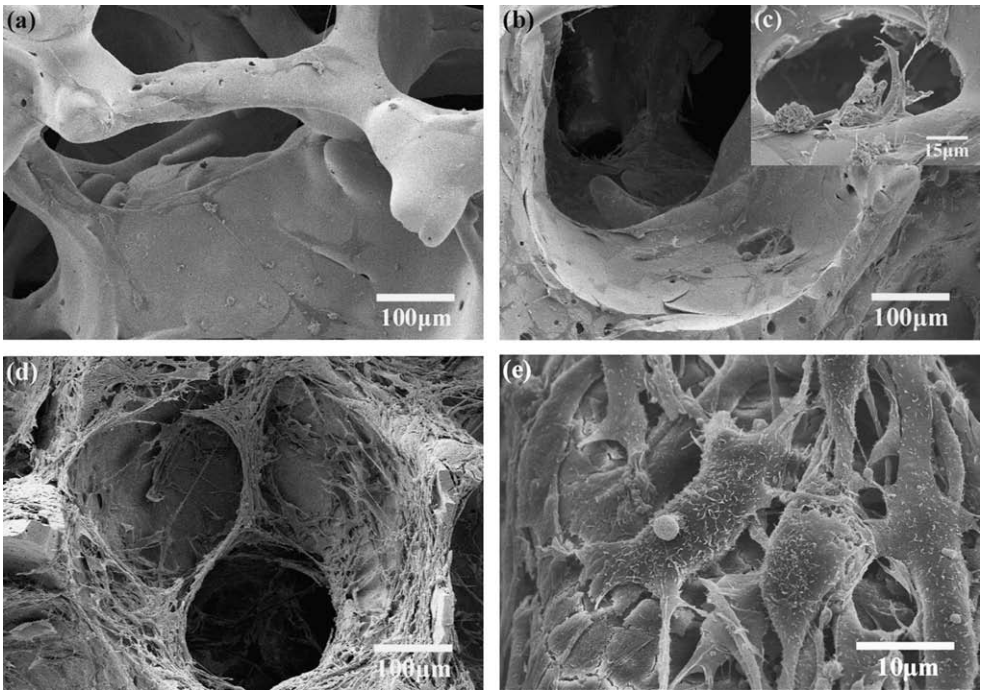

Fig. 9. SEM images of 13–93 glass scaffolds seeded with MC3T3-E1 cells and cultured for: (a) 2 days; (b, c) 4 days; and (d, e) 6 days.

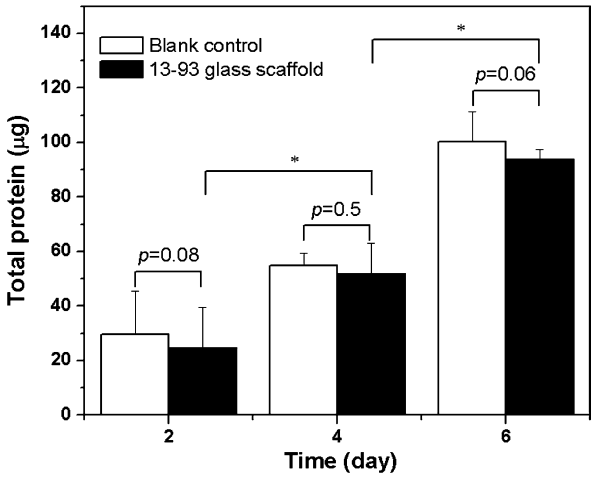

Fig. 10. Quantitative measurement of total protein content per scaffold or well in MC3T3-E1 cell cultures incubated for 2, 4 and 6 days on 13–93 glass scaffolds and in control wells. Mean ± sd; $n = 4$. *Significant increase in the total amount of protein on the porous 13–93 glass scaffolds with increasing culture duration ($p < 0.05$).

within the interior of the constructs indicated that the pore network had good interconnectivity.

4. Discussion

The colloid stability of the suspension is critical for achieving homogeneous particle packing in the construct formed by the polymer foam infiltration technique, and therefore for achieving a fully dense solid network during sintering. By optimizing the suspension characteristics and heating schedule, 13–93 glass scaffolds with a porosity of 85 ± 2% and pores of size 100–500 μm were produced. The use of a selected polymer foam resulted in the production of constructs with a microstructure approximating that of trabecular bone (Fig. 4).

The compressive strength of the fabricated 13–93 glass constructs (11 ± 1 MPa) was approximately equal to the highest compressive strength reported for trabecular bone (2–12 MPa) [42,43]. The mechanical behavior of cellular solids with open-cells has been described by the Gibson and Ashby model [35]. According to the model, the compressive strength σ_{cr} of brittle cellular foams (ceramic or glass) is given by

$$\frac{\sigma_{cr}}{\sigma_{fs}} = C_1\left(\frac{\rho}{\rho_0}\right)^{3/2}\frac{1+(t_i/t)^2}{\sqrt{1-(t_i/t)^2}} = C_1(1-P)^{3/2}\frac{1+(t_i/t)^2}{\sqrt{1-(t_i/t)^2}} \quad (2)$$

where σ_{fs} is the modulus of rupture of the struts of the foam, C_1 is a constant of proportionality, ρ and ρ_0 are the densities of the foam and the fully dense solid, respectively, P is the porosity of the foam and t_i/t is the ratio of the central void size of the struts to the strut size. The modulus of rupture in bending is the maximum stress at failure. For 13–93 glass fibers with a diameter of 50–100 μm, the tensile strength has been reported as 650 ± 390 MPa [44]. The diameter of the struts in the sintered 13–93 glass scaffolds was in the range 50–100 μm, so the modulus of rupture of the struts was estimated as the tensile strength of the 13–93 glass fibers. For brittle cellular foams, $C_i = 0.2$ [35]. The struts in the present work were almost fully dense,

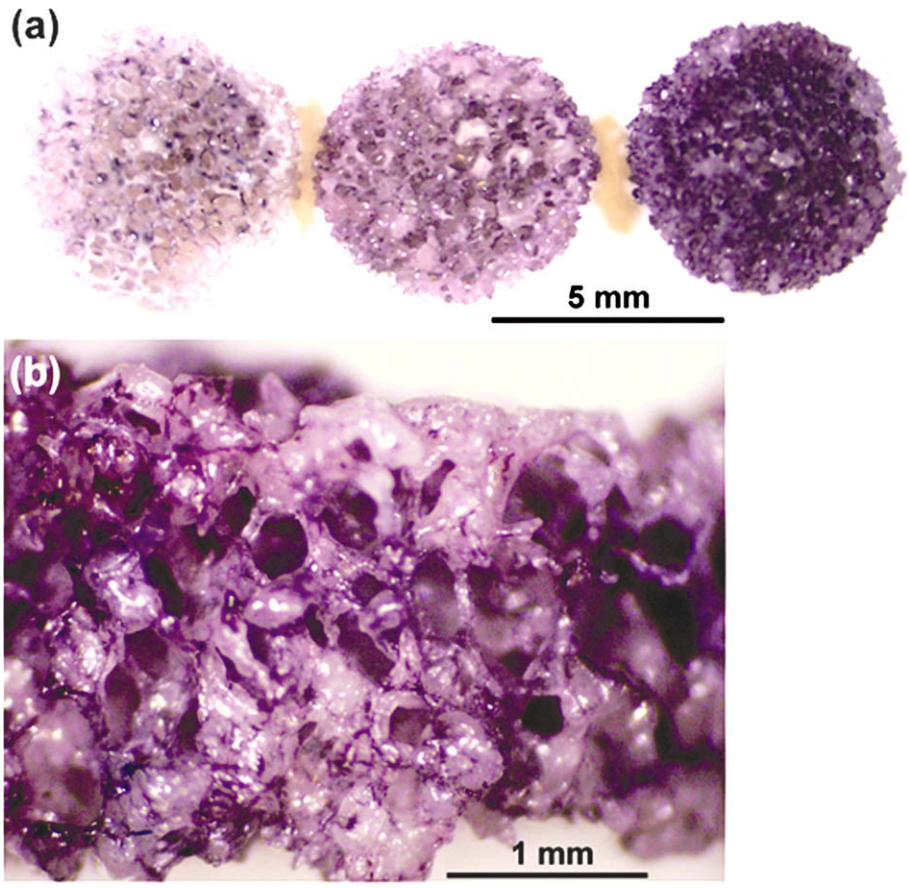

Fig. 11. Cell-seeded 13–93 glass scaffolds treated with MTT: (a) surface of scaffolds after culture intervals of 2, 4 and 6 days (left to right, respectively); and (b) freeze-fracture section of scaffold cultured for 6 days, showing clusters of MTT-labeled cells within the interior.

so $t_i/t = 0$. Based on these values, the compressive strength of the 13–93 glass scaffolds ($P = 0.83$–0.87) was predicted to be 2–15 MPa, which is the same order of magnitude as the measured compressive strength (11 ± 1 MPa).

The measured compressive strength of the 13–93 glass constructs was at least one order of magnitude higher than the values reported for biodegradable polymer scaffolds or polymer–ceramic composites prepared by the TIPS method or by the gas foaming method [5,20,45,46]. The strength was also considerably higher than the values reported for bioactive glass–ceramic and HA constructs with similar porosity, which were produced by a polymer foam replication technique. Glass–ceramic constructs formed from bioactive 45S5 glass had a compressive strength of 0.3–0.4 MPa (porosity = 89–92%) [15] and constructs formed from a calcium phosphate glass had a compressive strength of 0.8–1.4 MPa [47]. HA constructs had compressive strengths of 0.01–0.2 MPa (porosity = 86%) [29], 0.2 MPa (porosity = 86%) [48] and 0.6–5.0 MPa (porosity = 70–77%) [30], while HA constructs coated with apatite–wollastonite glass ceramic had a compressive strength of ~1 MPa (porosity = 93%) [49]. A higher compressive strength of 17 MPa (porosity = 73%) was obtained for HA constructs prepared by a gas foaming technique [50], whereas a much higher strength (30 ± 8 MPa) was obtained for HA constructs formed by a solid freeform fabrication (or rapid prototyping) technique but the porosity of the constructs was only 35% [51].

When compared to constructs prepared by the polymer foam replication technique, the higher strength achieved in the present work was attributed to two reasons: (i) the homogeneous particle packing in the as-formed constructs, which facilitated the densification of the particulate network during sintering; and (ii) the ease of densifying the particulate network during sintering, due to the favorable viscous flow characteristics of 13–93 glass. In comparison, 45S5 glass suffers from limited viscous flow and the glass crystallizes prior to densification, so full densification of the particulate network of the construct is difficult. In the polymer foam replication technique, decomposition of the polymer results in the formation of triangular voids in the particulate network [52]. In glass–ceramics and crystalline ceramics such as HA, these triangular voids, much larger than the particle size of the material, are difficult to remove during the sintering stage because of the limited viscous flow or diffusion in these materials. This residual porosity in the solid network of the cellular structure leads to a reduction in strength. The triangular voids in the

constructs fabricated in this work were filled by facile viscous flow of the 13–93 glass during sintering, giving a dense solid network with higher strength.

The elastic modulus of the fabricated 13–93 glass scaffolds was 3.0 ± 0.5 GPa, approximately equal to the upper limit of values reported for human trabecular bone (0.1–5 GPa) [36]. The elastic modulus of cellular low-density solids is given by [35]:

$$\frac{E}{E_0} = C_2\left(\frac{\rho}{\rho_0}\right)^n = C_2(1-P)^n \quad (3)$$

where E and E_0 are the elastic modulus values of the porous cellular material and the fully dense solid, respectively, C_2 and n are constants that depend on the microstructure, and C_2 includes all geometric constants of proportionality. For cellular structures with a dense solid network, $C_2 = 1$, whereas in the case of a hollow ceramic network with a central void, $C_2 = 0.3$. The constant n has a value in the range $1 < n < 4$, with $n = 2$ for open-cell structures. Microstructural observations (Fig. 4) indicated that the fabricated 13–93 constructs can be approximated as an open-cell structure in which the solid network was fully dense. In this case, $C_2 = 1$ and $n = 2$. The elastic modulus of dense silicate glass is 60–80 GPa [53]. Using these values, and the measured porosity of the fabricated glass constructs ($P = 0.83$–0.87), the elastic modulus E of the porous glass scaffold is predicted to be 1.0–2.3 GPa, which is within a factor of 2 of the measured value (3.0 ± 0.5 GPa).

The formation of a biologically active HA layer, which is equivalent chemically and structurally to the main mineral constituent of bone, is a key requirement for developing a strong interfacial bond between bioactive ceramics and tissues in vivo [9]. The formation of an HA surface layer in vitro is indicative of a material's bioactive potential in vivo [3]. In the present work, the formation of an HA surface layer was observed within 7 days for the 13–93 glass immersed in an SBF (Fig. 7). The HA crystals were similar to those of human trabecular bone in terms of size, morphology and chemical composition. In comparison, the formation of an amorphous calcium phosphate layer on the surface of porous 45S5 glass–ceramic constructs was observed after 28 days in an SBF [15]. More rapid formation of an HA layer is favorable for obtaining early biological fixation of a bioactive implant in bone repair and regeneration.

The MC3T3-E1 cells are a well-characterized mouse preostoblastic cell line, and they have been used widely for in vitro cytotoxicity testing of biomaterials [36,37]. The M3T3-E1 cell morphology on the porous 13–93 glass scaffolds in this work was similar to that observed on 45S5 glass discs reported elsewhere [54]. The cells colonized the surfaces of the porous 13–93 glass scaffolds, and aggregated with each other. The cell morphology, coupled with the in vitro cell culture data, indicated the ability of the 13–93 glass scaffolds to support the attachment and proliferation of MC3T3-E1 osteoblastic cells, both on the surface and within the interior of the porous constructs (Figs. 9–11). This, coupled with the favorable pore characteristics, microstructure, in vitro bioactivity and compressive mechanical properties, indicates the potential of the fabricated 13–93 glass constructs for eventual application in bone repair and regeneration. Additional work is presently underway to assess the ability of the 13–93 glass scaffolds to support the production of extracellular matrix and bone mineralization in vitro.

5. Conclusions

Scaffolds of 13–93 bioactive glass, with a porosity of $85 \pm 2\%$ and pores of size 100–500 μm, were fabricated with a microstructure similar to that of trabecular bone using a polymer foam replication technique. The constructs had a compressive strength of 11 ± 1 MPa and an elastic modulus of 3.0 ± 0.5 GPa, equal to the highest values reported for human trabecular bone. Upon immersion in a simulated body fluid, a nanostructured hydroxyapatite layer formed on the surface of the porous scaffolds within 7 days, indicating the in vitro bioactivity of the scaffolds. In vitro cell culture and SEM observations showed that the scaffolds had an excellent ability to support the attachment and subsequent proliferation of MC3T3-E1 preosteoblastic cells, both on the surface and in the interior of the constructs. The results suggest that the fabricated 13–93 glass scaffolds could be applied as biological scaffolds for osseous repair and regeneration.

References

[1] Goldstein SA, Patil PV, Moalli MR. Perspectives on tissue engineering of bone. Clin Orthop 1999;357S:S419–23.
[2] Kneser U, Schaefer DJ, Munder B, Klemt C, Andree C, Stark GB. Tissue engineering of bone. Min Invas Ther Allied Technol 2002;11:107–16.
[3] Griffith LG. Polymeric biomaterials. Acta Mater 2000;48:263–77.
[4] Borden M, El-Almin SF, Attawia M, Laurencin CT. Structural and human cellular assessment of a novel microsphere-based tissue engineered scaffold for bone repair. Biomaterials 2003;24:597–609.
[5] Zhang R, Ma PX. Poly(α-hydroxyl acids)/hydroxyapatite porous composites for bone tissue engineering. I. Preparation and morphology. J Biomed Mater Res 1999;44:446–55.
[6] Thomson RC, Yaszemski MJ, Powers JM, Mikos AG. Hydroxyapatite fiber-reinforced poly(α-hydroxy ester) foams for bone regeneration. Biomaterials 1998;19:1935–43.
[7] Roether JA, Gough GE, Boccaccini AR, Hench LL, Maquet V, Jerôme R. Novel bioresorbable and bioactive composites based on bioactive glass and polylactide foams for bone tissue engineering. J Mater Sci: Mater Med 2002;13:1207–14.
[8] Hench LL, Wilson J. Surface active biomaterials. Science 1984;226:630–6.
[9] Hench LL. Bioceramics. J Am Ceram Soc 1998;81:1705–28.
[10] Huang W, Day DE, Kittiratanapiboon K, Rahaman MN. Kinetics and mechanisms of the conversion of silicate (45S5), borate, and borosilicate glasses to hydroxyapatite in dilute phosphate solutions. J Mater Sci: Mater Med 2006;17:583–96.
[11] Huang W, Rahaman MN, Day DE, Li Y. Mechanisms of converting silicate, borate, and borosilicate glasses to hydroxyapatite in dilute phosphate solution. Phys Chem Glasses: Eur J Glass Sci Technol B 2006;47:647–58.

[12] Rahaman MN, Brown RF, Bal BS, Day DE. Bioactive glasses for non-bearing applications in total joint replacement. Semin Arthroplast 2007;17:102–12.
[13] Fu Q, Rahaman MN, Bal BS, Huang W, Day DE. Preparation and bioactive characteristics of a porous 13–93 glass, and fabrication into the articulating surface of a proximal tibia. J Biomed Mater Res 2007;82A:222–9.
[14] Filho OP, LaTorr GP, Hench LL. Effect of crystallization on apatite-layer formation on bioactive glass 45S5. J Biomed Mater Res 1996;30:509–14.
[15] Chen ZQ, Thompson ID, Boccaccini AR. 45S5 Bioglass®-derived glass–ceramic scaffold for bone tissue engineering. Biomaterials 2006;27:2414–25.
[16] Brink M. The influence of alkali and alkali earths on the working range for bioactive glasses. J Biomed Mater Res 1997;36:109–17.
[17] Brink M, Turunen T, Happonen R, Yli-Urppo A. Compositional dependence of bioactivity of glasses in the system Na_2O–K_2O–MgO–CaO–B_2O_3–P_2O_5–SiO_2. J Biomed Mater Res 1997;37:114–21.
[18] Brown RF, Day DE, Day TE, Jung S, Rahaman MN, Fu Q. Growth and differentiation of osteoblastic cells on 13-93 bioactive glass fibers and scaffolds. Acta Biomater 2008;4:387–96.
[19] Maquet V, Boccaccini AR, Pravata L, Notingher I, Jérôme R. Preparation, characterization, and in vitro degradation of bioresorbable and bioactive composites based on Bioglass-filled polylactide foams. J Biomed Mater Res A 2003;66A:335–46.
[20] Ma PX, Zhang R. Microtubular architecture of biodegradable polymer scaffolds. J Biomed Mater Res 2001;56:469–77.
[21] Dellinger JG, Cesarano III J, Jamison RD. Robotic deposition of model hydroxyapatite scaffolds with multiple architectures and multiscale porosity for bone tissue engineering. J Biomed Mater Res A 2007;82A:383–94.
[22] Lin CY, Wirtz T, LaMarca F, Hollister SJ. Structural and mechanical evaluations of a topology optimized titanium interbody fusion cage fabricated by selective laser melting process. J Biomed Mater Res A 2007;83A:272–9.
[23] Lu HH, El-Amin SF, Scott KD, Laurencin CT . Three-dimensional, bioactive, biodegradable, polymer-bioactive glass composite scaffolds with improved mechanical properties support collagen synthesis and mineralization of human osteoblast-like cells in vitro. J Biomed Mater Res A 2003;64A:465–74.
[24] Kim SS, Ahn KM, Park MS, Lee JH, Choi CY, Kim BS. A poly(lactide-co-glycolide)/hydroxyapatite composite scaffold with enhanced osteoconductivity. J Biomed Mater Res A 2007;80A:206–15.
[25] Deville S, Saiz E, Tomsia A. Freeze casting of hydroxyapatite scaffolds for bone tissue engineering. Biomaterials 2006;27:5480–9.
[26] Deville S, Saiz E, Nalla RK, Tomsia A. Freezing as a path to build complex composites. Science 2006;311:515–8.
[27] Fu Q, Rahaman MN, Dogan F, Bal BS. Freeze casting of porous hydroxyapatite scaffolds – I. Processing and general microstructure. J Biomed Mater Res B: Appl Biomater [in press].
[28] Fu Q, Rahaman MN, Dogan F, Bal BS. Freeze casting of porous hydroxyapatite scaffolds – II. Sintering, microstructure, and mechanical properties. J Biomed Mater Res B: Appl Biomater [in press].
[29] Callcut S, Knowles JC. Correlation between structure and compressive strength in a reticulate glass-reinforced hydroxyapatite foam. J Mater Sci Mater Med 2002;13:485–9.
[30] Ramay HRR, Zhang M. Preparation of porous hydroxyapatite scaffolds by combination of the gel-casting and polymer sponge methods. Biomaterials 2003;24:3293–302.
[31] Ramay HRR, Zhang M. Biphasic calcium phosphate nanocomposite porous scaffolds for load-bearing bone tissue engineering. Biomaterials 2004;25:5171–80.
[32] Wu C, Chang J, Zhai W, Ni S, Wang J. Porous akermanite scaffolds for bone tissue engineering: preparation, characterization, and in vitro studies. J Biomed Mater Res B: Appl Biomater 2006;78B:47–55.
[33] Hulbert SF, Young FA, Mathews RS, Klawitter JJ, Talbert CD, Stelling FH. Potential of ceramic materials as permanently implantable skeletal prostheses. J Biomed Mater Res 1970;4:433–56.
[34] Hollinger JO, Brekke J, Gruskin E, Lee D. Role of bone substitutes. Clin Orthop Relat Res 1996;324:55–65.
[35] Gibson LJ, Ashby MF. Cellular solids: structure and properties. 2nd ed. Cambridge: Cambridge University Press; 1997.
[36] Foppiano S, Marshall SJ, Marshall GW, Saiz E, Tomsia AP. The influence of novel bioactive glasses on in vitro osteoblast behavior. J Biomed Mater Res A 2004;71A:242–9.
[37] Inoue M, LeGeros RZ, Inoue M, Tsujigiwa H, Nagatsuka H. In vitro response of osteoblast-like and odontoblast-like cells to unsubstituted and substituted apatites. J Biomed Mate Res A 2004;70A:585–93.
[38] Rahaman MN. Ceramic processing. Boca Raton (FL): Taylor & Francis/CRC Press; 2006.
[39] Kokubo T, Kushitani H, Sakka S, Kitsugi T, Yamamuro T. Solutions able to reproduce in vivo surface-structure changes in bioactive glass–ceramic A–W. J Biomed Mater Res 1990;24:721–34.
[40] Krieger IM, Dougherty M. A mechanism for non-newtonian flow in suspensions of rigid spheres. Trans Soc Rheol 1959;3:137–52.
[41] Bergström L. Shear thinning and shear thickening of concentrated ceramic suspensions. Colloids Surf A: Physicochem Eng Aspec 1998;133:151–5.
[42] Carter DR, Hayes WC. Bone compressive strength: the influence of density and strain rate. Science 1976;194:1174–6.
[43] Fung YC. Biomechanics: mechanical properties of living tissues. New York: Springer; 1993.
[44] Pirhonen E, Niirannen H, Niemelä, Brink M, Törmälä P. Manufacturing, mechanical characterization, and in vitro performance of bioactive glass 13–93 fibers. J Biomed Mater Res B: Appl Biomater 2006;77B:227–33.
[45] Yang F, Qu X, Cui W, Bei J, Yu F, Lu S, et al. Manufacturing and morphology structure of polylactide-type microtubular orientation-structure scaffolds. Biomaterials 2006;27:4923–33.
[46] Cyster LA, Grang DM, Howdle SM, Rose FRAJ, Irvine DJ, Freeman D, et al. The influence of dispersant concentration on the pore morphology of hydroxyapatite ceramics for bone tissue engineering. Biomaterials 2005;26:697–702.
[47] Park Y-S, Kim K-N, Kim K-M, Choi S-H, Kim C-K, Legeros RZ, et al. Feasibility of three-dimensional macroporous scaffold using calcium phosphate glass and polyurethane sponge. J Mater Sci 2006;41:4357–64.
[48] Kim HW, Knowles JC, Kim HE. Hydroxyapatite porous scaffold engineered with biological polymer hybrid coating for antibiotic vancomycin release. J Mater Sci Mater Med 2005;16:189–95.
[49] Jun I-K, Song J-H, Choi W-Y, Koh Y-H, Kim H-E. Porous hydroxyapatite scaffolds coated with bioactive apatite–wollastonite glass–ceramics. J Am Ceram Soc 2007;90:2703–8.
[50] Dong J, Kojima H, Uemura T, Kikuchi M, Tateishi T, Tanaka J. In vivo evaluation of a novel porous hydroxyapatite to sustain osteogenesis of transplanted bone marrow-derived osteoblastic cells. J Biomed Mater Res 2001;57:208–16.
[51] Chu T-MG, Orton DG, Hollister SJ, Feinberg SE, Halloran JW. Mechanical and in vivo performance of hydroxyapatite implants with controlled architectures. Biomaterials 2003;23:1283–93.
[52] Studart AR, Gonzenbach UT, Tervoort E, Gauckler LJ. Processing routes to macroporous ceramics: a review. J Am Ceram Soc 2006;89:1771–89.
[53] Rouxel T. Elastic properties of glasses: a multiscale approach. C R Mecanique 2006;334:743–53.
[54] Levy S, Dalen MV, Agonafer S, Soboyejo WO. Cell/surface interactions and adhesion on bioactive glass 45S5. J Mater Sci Mater Med 2007;18:89–102.